IEEE Access
Multidisciplinary | Rapid Review | Open Access Journal

Received December 15, 2018, accepted December 26, 2018, date of publication January 10, 2019, date of current version February 14, 2019.

Digital Object Identifier 10.1109/ACCESS.2019.2891768

Robust Nonlinear Controller Design for Damping of Sub-Synchronous Control Interaction in DFIG-Based Wind Farms

PENGHAN LI[1], JIE WANG[1], LINYUN XIONG[2], AND MEILING MA[1]
[1]School of Electronic Information and Electrical Engineering, Shanghai Jiao Tong University, Shanghai 200240, China
[2]School of Electrical Engineering, Chongqing University, Chongqing 400044, China

Corresponding authors: Jie Wang (jiewangxh@sjtu.edu.cn) and Linyun Xiong (1669554200@qq.com)

This work was supported by the National Natural Science Foundation of China under Grant 61374155.

ABSTRACT A robust controller taking advantage of feedback linearization control (FLC) and sliding mode control (SMC) is proposed with an objective of mitigating the sub-synchronous control interaction (SSCI) in series-compensated doubly fed induction generator (DFIG)-based wind farms (WFs). FLC method is employed to obtain the reduced-order model of the studied system and, hence, smaller computation burden to controller design. Moreover, unlike linear control methods, FLC enables the controlled system to be independent of the pre-specified operations, which is suitable for highly nonlinear DFIG-based WFs. Considering that the FLC can be sensitive to parameter uncertainties, SMC is combined with the FLC to improve the robustness of the system. To evaluate the performance of the proposed feedback-linearized sliding mode controller (FLSMC) as compared to the conventional sub-synchronous resonance damping controller, the electromagnetic transient simulation and small-signal stability analysis are carried out. The designed FLSMC is observed to demonstrate the effectiveness in SSCI mitigation and robustness against the parameter perturbation at varied operating conditions. The experimental tests are performed to validate the veracity of the simulation results.

INDEX TERMS Doubly fed induction generator, feedback linearization control, sliding mode control, sub-synchronous control interaction.

NOMENCLATURE

g, t	Subscript denoting generator and turbine
r, s	Subscript denoting rotor and stator
d, q	Subscript denoting direct and quadrature axes
rf, gf	Subscript denoting RSC filter and GSC filter
$*$	Superscript denoting reference value
ω_m, ω_1	Rotor shaft angular speed and system angular line frequency
$e_q, e_d; u_q, u_d$	Grid voltage and PCC voltage
u_{sc}	Voltage across series compensator
i_d, i_q	Current through transmissions
u_g, i_g	Voltage and current of the GSC loop
C_{sc}, R_L, L_L	Compensator capacitance, network equivalent resistance, and inductance
C_{dc}	DC-link capacitance
S_{gq}, S_{gd}	Switching signals for GSC

I. INTRODUCTION

Sub-synchronous control interaction (SSCI), a new class of sub-synchronous resonance (SSR), has received noteworthy attention in recent years [1], [2]. The first reported SSCI event occurred in ERCOT of USA [3], and was followed by incidents in Minnesota of USA [4], Hebei of China [5], and Xinjiang of China [6]. It is pointed out that SSCI effects can be amplified by the fast-acting control of DFIG converters [7]. Therefore, DFIG is more vulnerable to SSCI as compared to other types of wind turbine generators, such as permanent magnetic synchronous generator (PMSG) and self-excited induction generator (SEIG). Furthermore, since DFIG mechanical part is not engaged in SSCI, oscillations develop much faster than conventional SSR incidents [8].

Many efforts have been made to address the problem of SSCI [9]–[12]. Eigenvalue analysis and frequency scanning are widely employed to identify the existence of SSCI and explain its primary reason. FACTS devices are utilized for SSCI mitigation, including static VAR

compensator (SVC) [13], static synchronous compensator (STATCOM) [14], thyristor-controlled series compensator (TCSC) [15], distributed power flow controller (DPFC) [16], and unified power flow controller (UPFC) [17]. In addition, Nyquist stability criterion, residue analysis, and root locus are adopted to facilitate the implementation of the damping control for FACTS devices [18].

Nevertheless, considering the high cost of using FACTS devices, many researchers and engineers propose that SSCI mitigation can be achieved by exploiting the existing DFIG converter control. Advances have been produced in this area [16]–[20]. A lead-lag control block is added to the current control loop of rotor side converter (RSC) for DFIG to attenuate the oscillations due to SSCI [1]. With an observer to estimate the voltage of series capacitor, a supplementary controller is developed for grid side converter (GSC) control of DFIGs to alleviate SSCI [19]. Suppression filter is implanted to the converter control loop to deactivate SSCI in DFIG-based WFs interfaced with fixed series compensation, and the best location is identified using impedance model analysis [20]. To enhance system stability and damp SSCI, a two-degree-of-freedom control scheme is designed for DFIGs incorporating a damping controller [21]. For damping of SSCI in WFs, the authors develop a damping control scheme including a linear-quadratic regulator (LQR)-based state feedback controller and a full-state observer in [22]. Based on the linearized system model, a coordinated control scheme of SSCI damping controller and supplementary excitation damping controller is proposed for SSCI suppression in a practical power system in the north of China [23]. However, since these damping controllers are designed based on the linearized model of the DFIG-based WFs, satisfactory performance is guaranteed only within the pre-specified operating conditions. Therefore, feedback linearization control (FLC) method is employed in this paper to design a nonlinear controller for SSCI mitigation. With the use of FLC, the reduced-order model of the studied system is obtained and hence smaller computation burden to controller design. Moreover, unlike linear control methods, FLC enables the controlled system to be independent of pre-specified operations. Considering FLC can be sensitive to parameter uncertainties, a combined control scheme integrating FLC and sliding mode control (SMC) is hereby proposed. The major advantage of utilizing SMC is the insensitiveness to parameter perturbation [24]–[26]. To evaluate the effectiveness of the designed feedback-linearized sliding mode controller (FLSMC) as compared to conventional SSR damping controller (SSRDC), small-signal stability analysis and electromagnetic transient (EMT) simulation are carried out at varied compensation degrees and wind speeds. Furthermore, experimental tests are performed to validate the veracity of the simulation results.

The contributions of the paper are: (1) achieve feedback linearization of series-compensated DFIG-based WFs; (2) propose feedback-linearized sliding mode controller (FLSMC), which incorporates feedback linearization control and sliding mode control; (3) demonstrate the effectiveness of the proposed FLSMC in SSCI mitigation under varied operating conditions.

The remaining parts of the article is organized as follows. The model of series-compensated DFIG-based WF and conventional SSRDC are given in Section II. The design process of the FLSMC is presented in Section III. In Section IV, small-signal stability analysis, electromagnetic transient simulation, and experimental tests are performed to assess the effectiveness of the FLSMC. Section V concludes the article.

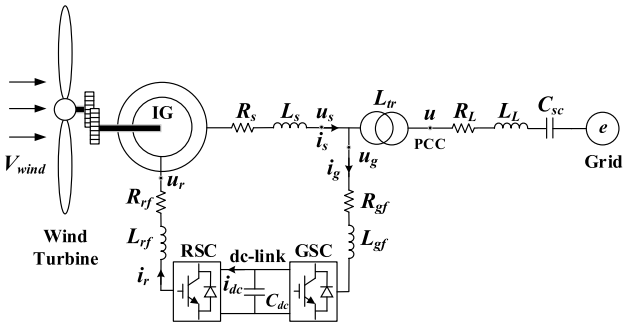

FIGURE 1. Series-compensated DFIG-based WF.

II. SYSTEM MODEL AND CONTROL

A. MATHEMATICAL MODELLING

As shown in Fig. 1, a 14th order model is adopted to describe the dynamics of the series-compensated DFIG-based WF, including wind turbine aerodynamics, shaft system, induction generator, dc-link, RSC, and GSC [27]. The studied system is expressed in the classical form of the nonlinear system as

$$\begin{cases} \dfrac{\mathrm{d}}{\mathrm{d}t}\boldsymbol{x} = \boldsymbol{f}(\boldsymbol{x}) + \boldsymbol{g}_1(\boldsymbol{x})\,u_1 + \boldsymbol{g}_2(\boldsymbol{x})\,u_2 \\ y_1 = h_1(\boldsymbol{x}) \\ y_2 = h_2(\boldsymbol{x}) \end{cases} \tag{1}$$

where $\boldsymbol{x} = [i_{gq}\, i_{gd}\, u_{dc}\, i_{rq}\, i_{rd}\, i_{sq}\, i_{sd}\, i_q\, i_d\, u_{scq}\, u_{scd}\ \ \omega_m\, \omega_r\, \gamma]^T$; $\boldsymbol{u} = [S_{gq}\, S_{gd}]^T$; $\boldsymbol{y} = [i_{gq}\, u_{dc}]^T$; the expressions of $g(\boldsymbol{x})$ and $f(\boldsymbol{x})$ are presented in Appendix.

B. SSRDC

A conventional SSRDC is adopted in this study for simulation comparison. As shown in Fig. 2, a damping control block is added to the control loop of GSC. Detailed design process of the SSRDC is presented in [19].

III. FEEDBACK-LINEARIZED SLIDING MODE CONTROLLER

A. FEEDBACK LINEARIZATION OF DFIG-BASED WF

The calculation of relative degree determines the system feedback linearizability. We can calculate

$$\begin{cases} L_{g_1} L_f^{1-1} h_1(\boldsymbol{x}) = L_{g_1} h_1(\boldsymbol{x}) = u_{dc}/L_{gf} \\ L_{g_2} L_f^{1-1} h_1(\boldsymbol{x}) = L_{g_2} h_1(\boldsymbol{x}) = 0 \end{cases} \tag{2}$$

$$\begin{cases} L_{g_1} L_f^{1-1} h_2(\boldsymbol{x}) = L_{g_1} h_2(\boldsymbol{x}) = 0 \\ L_{g_2} L_f^{1-1} h_2(\boldsymbol{x}) = L_{g_2} h_2(\boldsymbol{x}) = \left(i_{gq} S_{gq} + i_{gd} S_{gd}\right)/C_{dc} \end{cases} \tag{3}$$

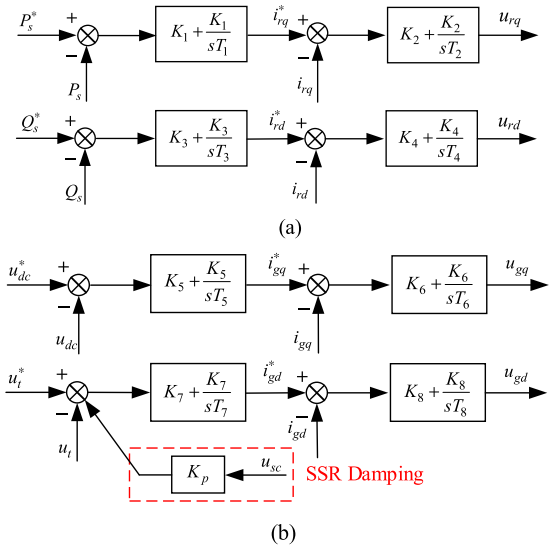

FIGURE 2. SSRDC: (a) RSC control; (b) GSC control.

where L denotes the Lie derivative. The calculations expressed by (2) and (3) indicate that the 2×2 matrix

$$\begin{bmatrix} L_{g_1}L_f^{1-1}h_1(\boldsymbol{x}) & L_{g_2}L_f^{1-1}h_1(\boldsymbol{x}) \\ L_{g_1}L_f^{1-1}h_2(\boldsymbol{x}) & L_{g_2}L_f^{1-1}h_2(\boldsymbol{x}) \end{bmatrix}$$

is nonsingular. The relative degree is $2 < 14$, which means the studied system is partially linearizable.

Therefore, the 14th order model decouples into two subsystems

$$\frac{\mathrm{d}}{\mathrm{d}t}\tilde{\boldsymbol{z}} = \tilde{\boldsymbol{A}}\tilde{\boldsymbol{z}} + \tilde{\boldsymbol{B}}\tilde{\boldsymbol{v}} \tag{4}$$

$$\frac{\mathrm{d}}{\mathrm{d}t}\hat{\boldsymbol{z}} = \hat{\boldsymbol{A}}\hat{\boldsymbol{z}} \tag{5}$$

where (5) denotes the transformed subsystem, $\tilde{\boldsymbol{z}}$ is new state variable; Equation (6) denotes the internal dynamics of the system, $\hat{\boldsymbol{z}}$ denotes the remaining states. For the studied system, we select

$$\begin{cases} \tilde{z}_1 = h_1(\boldsymbol{x}) = i_{gq} \\ \tilde{z}_2 = h_2(\boldsymbol{x}) = u_{dc} \end{cases} \tag{6}$$

then we have

$$\begin{cases} \dfrac{\mathrm{d}}{\mathrm{d}t}\tilde{z}_1 = \dfrac{\partial h_1(\boldsymbol{x})}{\partial \tilde{\boldsymbol{x}}}\dfrac{\mathrm{d}}{\mathrm{d}t}\boldsymbol{x} = -\omega_1 i_{gd} - \dfrac{R_{gf}}{L_{gf}}i_{gq} - \dfrac{u_{gq}}{L_{gf}} \\ \qquad\qquad + \dfrac{u_{dc}}{L_{gf}}u_1 \\ \dfrac{\mathrm{d}}{\mathrm{d}t}\tilde{z}_2 = \dfrac{\partial h_2(\boldsymbol{x})}{\partial \tilde{\boldsymbol{x}}}\dfrac{\mathrm{d}}{\mathrm{d}t}\boldsymbol{x} = \dfrac{1}{C_{dc}}i_{dc} - \dfrac{1}{C_{dc}}i_{gd}u_2 \\ \qquad\qquad - \dfrac{1}{C_{dc}}i_{gq}u_1 \end{cases} \tag{7}$$

Through utilizing linear control approach as $d\tilde{z}_i/dt = v_i$, the linearized form is obtained

$$\begin{cases} v_1 = -\omega_1 i_{gd} - \dfrac{R_{gf}}{L_{gf}}i_{gq} - \dfrac{u_{gq}}{L_{gf}} + \dfrac{u_{dc}}{L_{gf}}u_1 \\ v_2 = \dfrac{1}{C_{dc}}i_{dc} - \dfrac{1}{C_{dc}}i_{gq}u_1 - \dfrac{1}{C_{dc}}i_{gd}u_2 \end{cases} \tag{8}$$

where v_1 and v_2 denote the linear control inputs; physical control input u is computed from (8) as follows

$$\begin{cases} u_1 = \dfrac{L_{gf}}{u_{dc}}\left(v_1 + \omega_1 i_{gd} + \dfrac{R_{gf}}{L_{gf}}i_{gq} + \dfrac{u_{gq}}{L_{gf}}\right) \\ u_2 = -\dfrac{C_{dc}}{i_{gd}}\left(v_2 - \dfrac{i_{dc}}{C_{dc}} + \dfrac{L_{gf}i_{gq}}{C_{dc}u_{dc}}\right. \\ \qquad\qquad \left. \times \left(v_1 + \omega_1 i_{gd} + \dfrac{R_{gf}}{L_{gf}}i_{gq} + \dfrac{u_{gq}}{L_{gf}}\right)\right) \end{cases} \tag{9}$$

The internal dynamics stability is guaranteed using zero-dynamic theory, which is given in Appendix.

B. SMC BASED ON FEEDBACK LINEARIZATION

Define the sliding mode manifolds as

$$\boldsymbol{S} = \begin{bmatrix} S_1 \\ S_2 \end{bmatrix} = \begin{bmatrix} e_1 + c_1\int e_1 \\ e_2 + c_2\int e_2 \end{bmatrix} \tag{10}$$

where $e_1 = \tilde{z}_1 - \tilde{z}_1^* = i_{gq} - i_{gq}^*$, $e_2 = \tilde{z}_2 - \tilde{z}_2^* = u_{dc} - u_{dc}^*$; c_1 and c_2 are positive constants. Reference values i_{gq}^* and u_{dc}^* are computed from reference rotor active power P_r^* as [28]

$$\begin{cases} i_{gq}^* = \left(2P_r^*\right)/\left(3u_{gq}\right) \\ u_{dc}^* = P_r^*/i_{dc} \end{cases} \tag{11}$$

In the solution of $\dot{S} = 0$, equivalent control is derived

$$\begin{cases} v_{1eq} = -c_1 e_1 \\ v_{2eq} = -c_2 e_2 \end{cases} \tag{12}$$

To reduce the impact of parameter deviation, equivalent control is combined with reaching control as

$$\begin{cases} v_1 = v_{1eq} + v_{1s} = -c_1 e_1 - \varepsilon_1 sgnS_1 - k_1 S_1 \\ v_2 = v_{2eq} + v_{2s} = -c_2 e_2 - \varepsilon_2 sgnS_2 - k_2 S_2 \end{cases} \tag{13}$$

where $\varepsilon_1, \varepsilon_2, k_1, k_2$ are positive constants. Lyapunov function is chosen as

$$V = \frac{1}{2}\boldsymbol{S}^T\boldsymbol{S} \tag{14}$$

Time derivative of Lyapunov function is computed as

$$\begin{aligned} \dot{\boldsymbol{V}} &= \boldsymbol{S}^T\dot{\boldsymbol{S}} = S_1\left(\dot{e}_1 + c_1 e_1\right) + S_2\left(\dot{e}_2 + c_2 e_2\right) \\ &= S_1\left(-c_1 e_1 - \varepsilon_1 sgnS_1 - k_1 S_1 + c_1 e_1\right) \\ &\quad + S_2\left(-c_2 e_2 - \varepsilon_2 sgnS_2 - k_2 S_2 + c_2 e_2\right) \\ &= -\varepsilon_1|S_1| - k_1 S_1^2 - \varepsilon_2|S_2| - k_2 S_2^2 < 0 \end{aligned} \tag{15}$$

Therefore, the proposed FLSMC is asymptotically stable. Substituting (13) into (9), the control laws are obtained

$$\begin{cases} u_1 = \dfrac{L_{gf}}{u_{dc}}\left(-c_1 e_1 - \varepsilon_1 sgnS_1 - k_1 S_1\right. \\ \qquad\qquad \left. + \omega_1 i_{gd} + \dfrac{R_{gf}}{L_{gf}}i_{gq} + \dfrac{u_{gq}}{L_{gf}}\right) \\ u_2 = -\dfrac{C_{dc}}{i_{gd}}\left(-c_2 e_2 - \varepsilon_2 sgnS_2 - k_2 S_2 - \dfrac{i_{dc}}{C_{dc}}\right. \\ \qquad + \dfrac{L_{gf}i_{gq}}{C_{dc}u_{dc}}\left(-c_1 e_1 - \varepsilon_1 sgnS_1 - k_1 S_1\right. \\ \qquad \left.\left. + \omega_1 i_{gd} + \dfrac{R_{gf}}{L_{gf}}i_{gq} + \dfrac{u_{gq}}{L_{gf}}\right)\right) \end{cases} \tag{16}$$

The PI controller is adopted for GSC in this study [18].

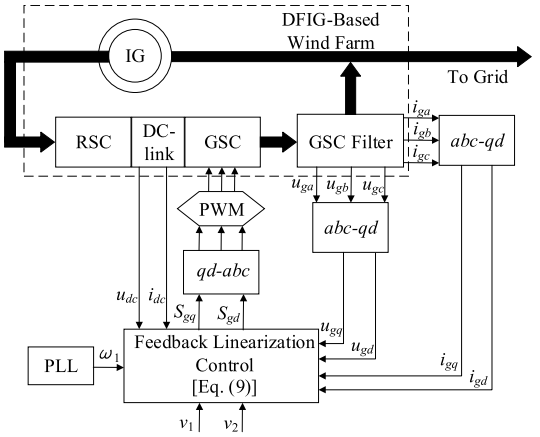

FIGURE 3. Block diagram of the feedback linearization control.

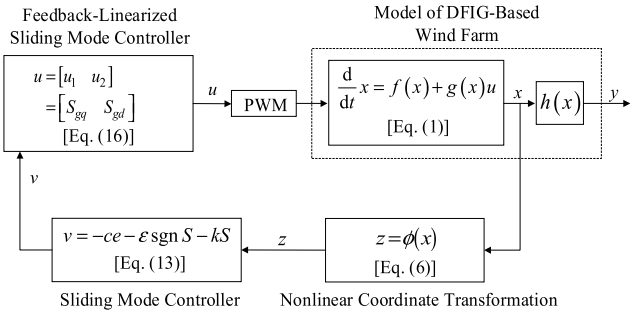

FIGURE 4. Block diagram of the proposed FLSMC.

IV. SIMULATION AND EXPERIMENTAL VALIDATION

The diagram of the FLC and FLSMC are illustrated in Figs. 3 and 4, respectively. It is observed that the new state variable z is obtained through nonlinear coordinate transformation expressed by (8). Then sliding mode controller expressed by (15) is designed based on the linear model of the studied system. Linear control signals and stator angular frequency are fed into the proposed controller to calculate the control laws. Eventually, pulse width modulator (PWM) is utilized for controller implementation.

A. SMALL-SIGNAL STABILITY ANALYSIS

1) SENSITIVITY ANALYSIS AND PARTICIPATION FACTORS

The eigenvalues for the studied system with the use of the designed controller are obtained using MATLAB function "linmod". In Table 1, λ_{15} to λ_{20} are nonoscillatory modes, $\lambda_{11,12}$ and $\lambda_{13,14}$ are related to PI controller in the converters, and $\lambda_{9,10}$ have a high frequency and a high damping. These modes are not further discussed [27]. From the characteristics and frequency range [18], $\lambda_{1,2}$ represent the sub-synchronous mode and $\lambda_{3,4}$ are super-synchronous mode. $\lambda_{5,6}$ are identified as electromechanical mode while $\lambda_{7,8}$ are shaft mode.

In this paper, the PI controller of GSC has been replaced by the proposed FLSMC, whereas RSC controller is implemented utilizing PI control. Considering the PI controllers could influence the performance of the damping controller, the sensitivity of the designed FLSMC to the PI controllers

TABLE 1. System modes at 7 m/s wind speed and 75% compensation level.

Mode	Eigenvalues	Mode	Eigenvalues
$\lambda_{1,2}$	-4.3±j126.2	λ_{15}	-103.8
$\lambda_{3,4}$	-10.6±j625.4	λ_{16}	-10.9
$\lambda_{5,6}$	-13.1±j99.2	λ_{17}	-9.1
$\lambda_{7,8}$	-0.9±j5.9	λ_{18}	-0.4
$\lambda_{9,10}$	-2501±j1258	λ_{19}	-20.1
$\lambda_{11,12}$	-0.2±j0.5	λ_{20}	-21.0
$\lambda_{13,14}$	-0.0		

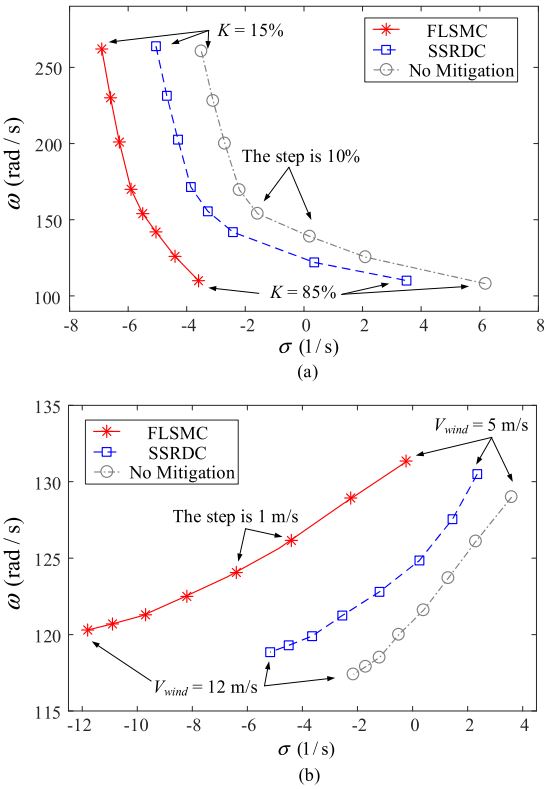

FIGURE 5. System eigenvalues: (a) at varied compensation levels 7 m/s wind speed; (b) at varied wind speeds 75% compensation level.

of RSC is studied using the following equation [29]

$$\frac{\partial \lambda_i}{\partial K_j} = \boldsymbol{\psi}_i \frac{\partial \boldsymbol{A}}{\partial K_j} \phi_i \tag{17}$$

where K_j ($j = 1, 2, 3, 4$) is the PI controller gains of RSC as illustrated in Fig. 2, $\boldsymbol{\psi_i}$ and $\boldsymbol{\phi_i}$ are the left and right eigenvectors, respectively, for eigenvalue λ_i. The computed eigenvalue sensitivities for the studied system are presented in Table 2. As demonstrated in Table 2, with the use of the FLSMC, the sensitivities of sub-synchronous mode ($\lambda_{1,2}$) with respect to PI controller gains of RSC are very small. However, it is observed that sub-synchronous mode is highly sensitive to the proportion gains K_2 and K_4 of RSC current tracking control when conventional SSRDC is adopted.

The participation factor is a measure of the relative participation of the kth variable in the ith mode of the system.

TABLE 2. Sensitivities to PI controller gains.

Eigenvalues	$\lambda_{1,2}$ (FLSMC)	$\lambda_{3,4}$ (FLSMC)	$\lambda_{5,6}$ (FLSMC)	$\lambda_{7,8}$ (FLSMC)	$\lambda_{1,2}$ (SSRDC)	$\lambda_{3,4}$ (SSRDC)	$\lambda_{5,6}$ (SSRDC)	$\lambda_{7,8}$ (SSRDC)
$\frac{\partial\lambda_i}{\partial K_1}$	0.0000	0.0000	0.0000	0.0000	0.0000	0.0000	0.0000	0.0000
$\frac{\partial\lambda_i}{\partial K_2}$	0.0021	0.0000	0.0000	0.0000	**0.2650**	0.0000	0.0000	0.0002
$\frac{\partial\lambda_i}{\partial K_3}$	0.0000	0.0000	0.0000	0.0000	0.0000	0.0001	0.0000	0.0000
$\frac{\partial\lambda_i}{\partial K_4}$	0.0011	0.0000	0.0000	0.0000	**0.1864**	0.0000	0.0000	0.0015

TABLE 3. System modes and participation factors.

	$\lambda_{1,2}$ -4.3±j126.2	$\lambda_{3,4}$ -10.6±j625.4	$\lambda_{5,6}$ -13.1±j99.2	$\lambda_{7,8}$ -0.9±j5.9
d-axis stator current i_{sd}	**0.2062**	**0.1654**	**0.1896**	0.0871
q-axis stator current i_{sq}	**0.2688**	**0.2105**	**0.2678**	0.0028
d-axis rotor current i_{rd}	**0.2065**	**0.1588**	**0.2074**	**0.1025**
q-axis rotor current i_{rq}	**0.2650**	**0.1984**	**0.2803**	0.0032
d-axis capacitor voltage u_{scd}	0.0058	0.0578	0.0011	0.0000
q-axis capacitor voltage u_{scq}	0.0062	0.0624	0.0015	0.0020
d-axis line current i_d	0.0045	0.0486	0.0016	0.0051
q-axis line current i_q	0.0040	0.0465	0.0013	0.0000
rotor speed ω_r	0.0005	0.0000	0.0012	**0.3021**
turbine speed ω_t	0.0000	0.0000	0.0000	0.0653
torque between two masses T_g	0.0000	0.0000	0.0000	**0.3748**
dc-link voltage u_{dc}	0.0000	0.0002	0.0000	0.0000
PI control gains of RSC K_1	0.0000	0.0000	0.0000	0.0000
PI control gains of RSC K_2	0.0000	0.0000	0.0000	0.0002
PI control gains of RSC K_3	0.0000	0.0000	0.0000	0.0000
PI control gains of RSC K_4	0.0000	0.0000	0.0000	0.0145

The magnitude of the normalized participation factors for an eigenvalue, i.e. λ_i is defined as [29]

$$p_{ki} = \phi_{ki}\psi_{ik} \tag{18}$$

where p_{ki} is the participation factor. Table 3 presents eigenvalues and participation factors under FLSMC at 75% compensation level and 7 m/s wind speed. In the table, larger participation factors in each column are bolded. From the table, it is observed that $\lambda_{1,2}$, $\lambda_{3,4}$, and $\lambda_{5,6}$ are closely related to the currents of stator and rotor, i.e., i_{sd}, i_{sq}, i_{rd}, and i_{rq}. Furthermore, the rotor speed (ω_r) and torque between the two masses (T_g) have higher participation in $\lambda_{7,8}$ (shaft mode). It is also seen that the parameters of PI controller of RSC have little impact on system modes.

2) EIGENVALUE ANALYSIS

To investigate the effect of wind speed and compensation level on system stability, eigenvalues at different operating conditions are shown in Fig. 5. It is observed that the increase in compensation degrees or the decrease in wind speeds undermines the stability of DFIG-based WF. Furthermore, unlike SSRDC, the proposed FLSMC can stabilize the studied system even at low wind speeds and high compensation levels.

B. ELECTROMAGNETIC TRANSIENT SIMULATION

Simulation model with PSCAD/EMTDC is shown in Fig. 6.

Fig. 6(a) shows the model of control law u_1 (S_{gq}), where corresponding SMC is encapsulated in "SMC" module. After *qd-abc* transformation, PWM is employed to generate GSC driving signals as illustrated in Fig. 6(b) and 6(c).

EMT simulation is performed at 7 m/s wind speed, and 75% compensation level is applied to transmissions at $t = 1$ s. System responses are presented in Fig. 7, including active power of transmissions and PCC voltage. In Fig. 7, the waveforms exhibit the effectiveness of FLSMC and SSRDC in suppressing SSCI, and FLSMC shows better performance. It is seen that oscillations due to SSCI are mitigated in less time under the proposed FLSMC.

As shown in Fig. 8, EMT simulation is repeated at 45% compensation level and 7 m/s wind speed. It is observed that SSCI problem is less severe with the decrease in

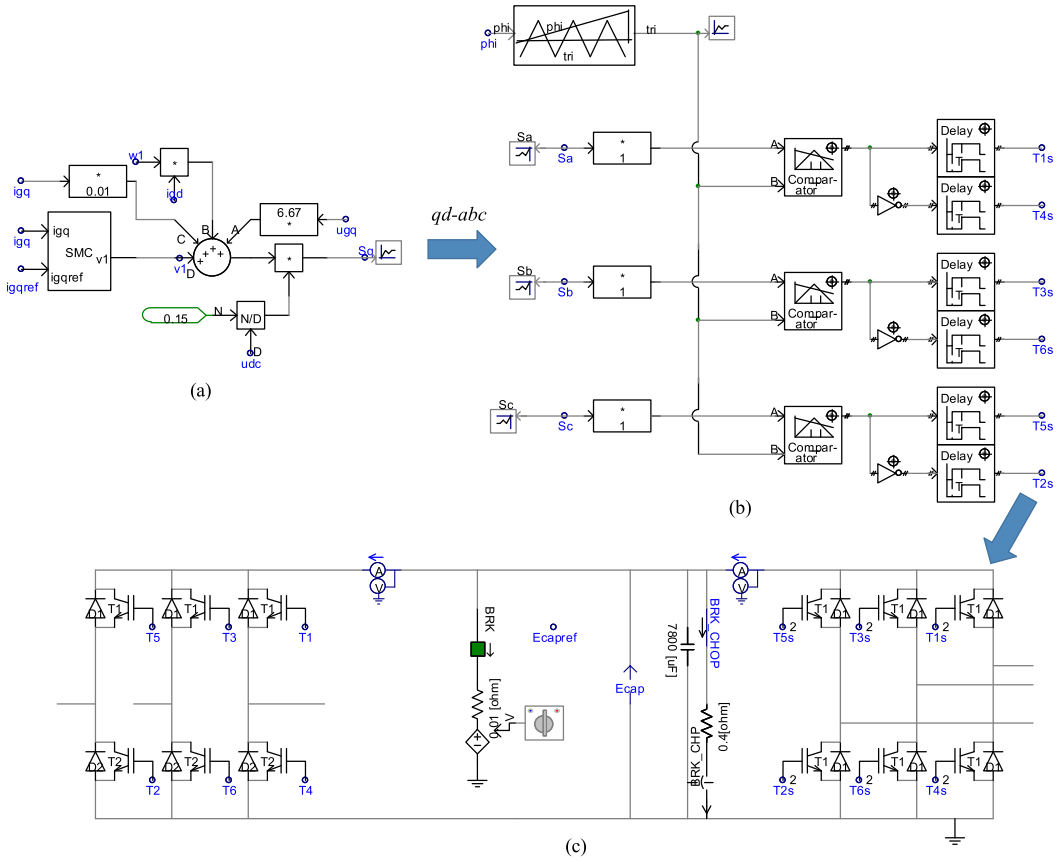

FIGURE 6. Simulation model: (a) control law S_q; (b) Circuit of GSC driving signals; (c) PWM.

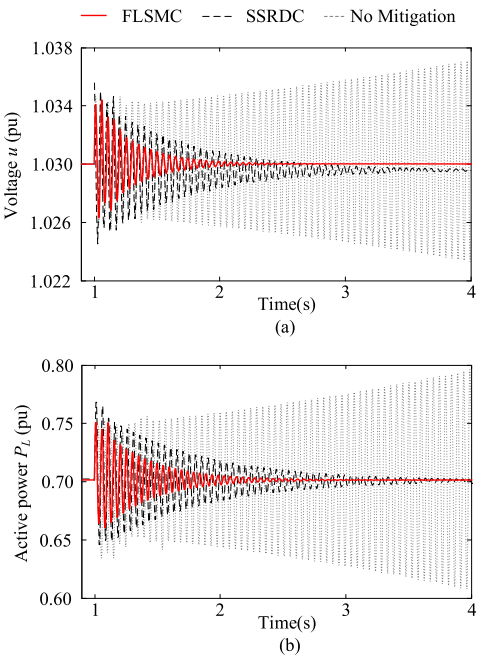

FIGURE 7. System responses for 75% series-compensation and 7 m/s wind speed: (a) PCC voltage; (b) transmission line active power.

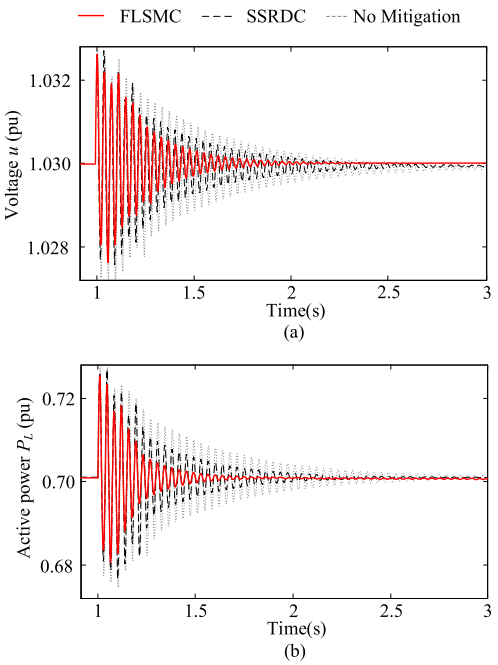

FIGURE 8. System responses for 45% series-compensation and 7 m/s wind speed: (a) PCC voltage; (b) transmission line active power.

compensation levels. Additionally, the oscillation frequency becomes higher at lower compensation levels. Both observations are consistent with the conclusion drawn by eigenvalue analysis.

To evaluate the performance of the controllers quantitatively, three performance indexes are adopted as follows

$$\mathrm{PI}_1 = \sup_{t\in[0,t_{sim}]} |e(t)| \tag{19}$$

TABLE 4. Performance indexes.

Cases/Performance index		PI_1	PI_2	PI_3
K: 75% V_w: 5 m/s	SSRDC	0.5424	0.7120	0.0636
	FLSMC	0.3201	0.2375	0.0389
K: 45% V_w: 5 m/s	SSRDC	0.2755	0.2295	0.0324
	FLSMC	0.1820	0.1026	0.0212

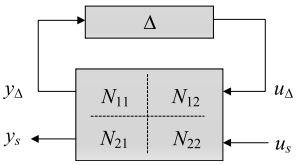

FIGURE 9. Uncertain model expressed in LFT form.

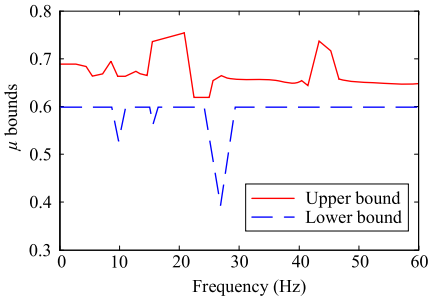

FIGURE 10. The μ-curves of the system with the FLSMC.

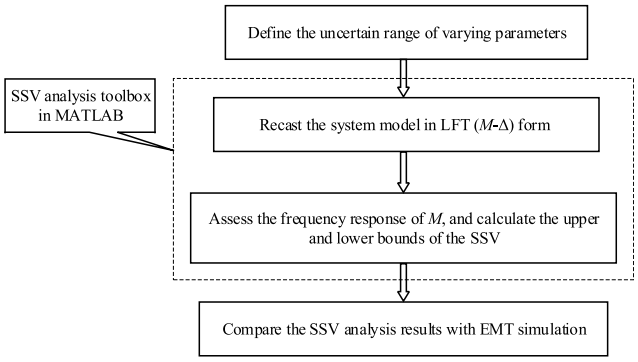

FIGURE 11. Procedure of evaluating robust stability.

$$\mathrm{PI}_2 = \int_0^{t_{sim}} |e(t)|\, dt \tag{20}$$

$$\mathrm{PI}_3 = \sqrt{\frac{\sum_{i=1}^{N} (e_i - \bar{e})^2}{N-1}} \tag{21}$$

where the sum of the electromechanical torque, d-axis rotor current, and dc-link voltage is taken as the error signal; PI_1 denotes the maximal absolute value of tracking errors during the simulation time (t_{sim}); PI_2 denotes the integral of absolute tracking errors; PI_3 denotes the standard deviations of the tracking errors, N represents the number of observations in the sample. The performance indexes for different simulated cases are listed in Table 4. It is observed that, for both cases, the FLSMC has lower value than the conventional SSRDC,

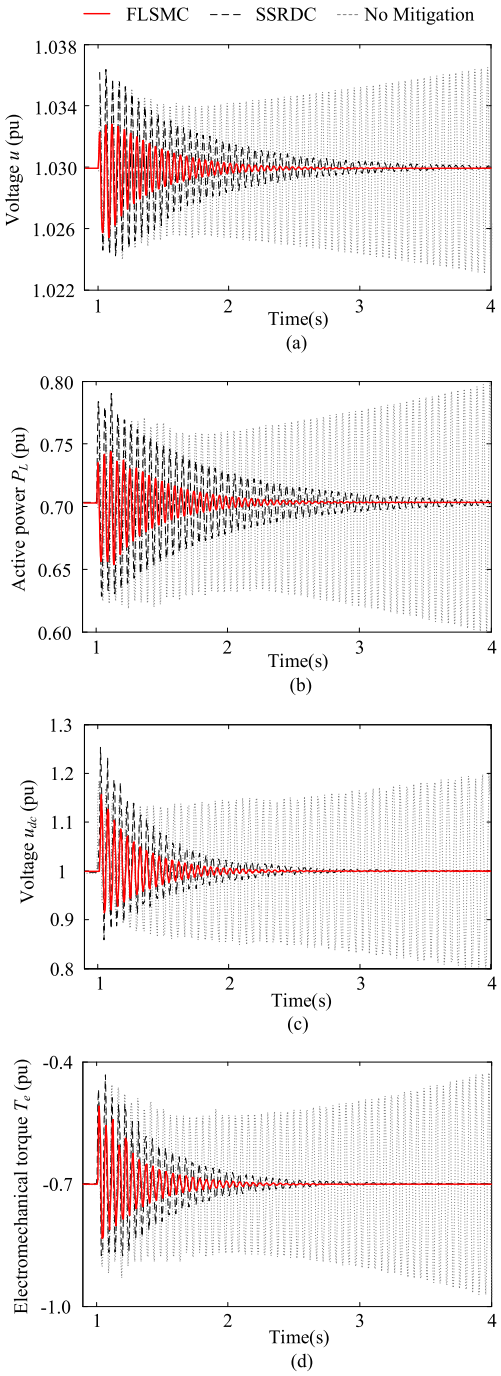

FIGURE 12. System responses with +20% variation in R_{gf} and L_{gf} for 75% series-compensation and 7 m/s wind speed: (a) PCC voltage; (b) transmission line active power; (c) dc-link voltage; (d) electromechanical torque.

which demonstrates the superior damping performance of the proposed controller.

C. ROBUST STABILITY ANALYSIS

Structured singular value (SSV) analysis is carried out to evaluate the robust stability of the FLSMC under parameter perturbations. The system model should be transformed into linear fractional transformation (LFT) form for SSV analysis

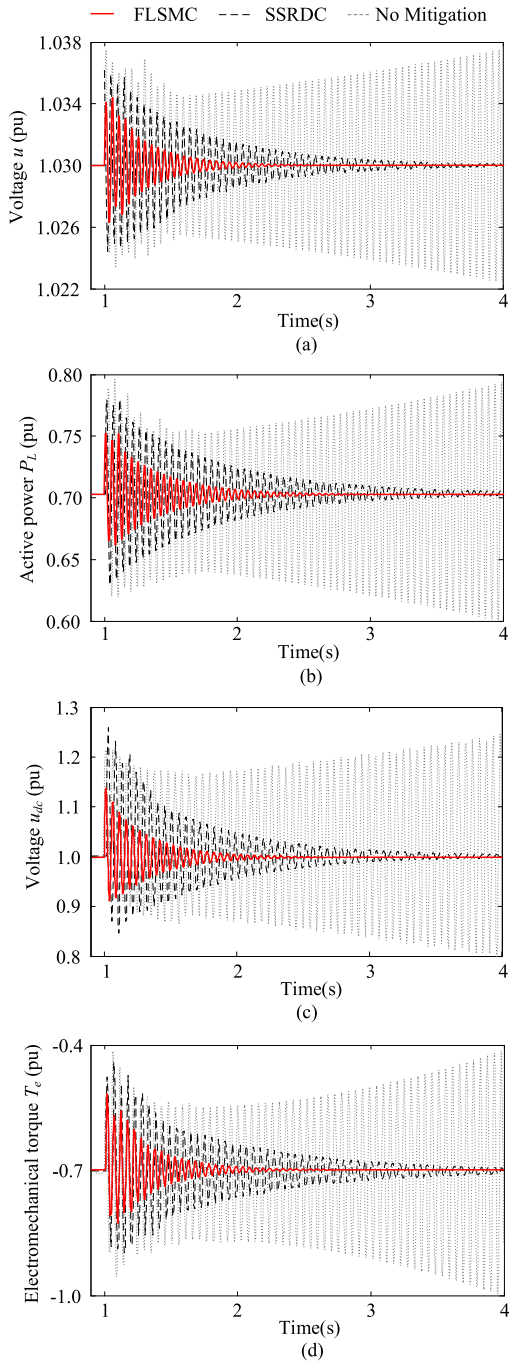

FIGURE 13. System responses with −20% variation in R_{gf} and L_{gf} for 75% series-compensation and 7 m/s wind speed: (a) PCC voltage; (b) transmission line active power; (c) dc-link voltage; (d) electromechanical torque.

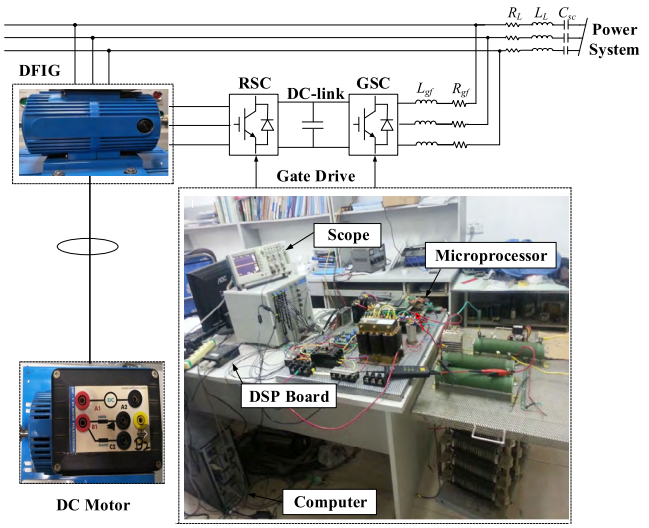

FIGURE 14. Experimental setup.

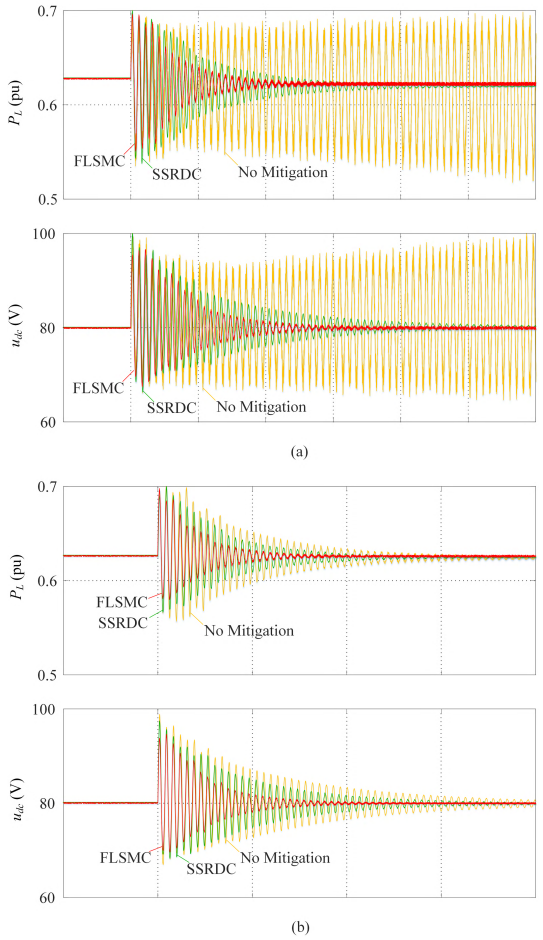

FIGURE 15. Experimental results: (a) 75% compensational level; (b) 45% compensational level. (t = 500 ms/div).

as shown in Fig. 9, where matrix Δ includes the set of uncertainties (±20% in R_{gf} and L_{gf}). General LFT expression is as follows

$$F_u(N, \Delta) = \frac{y_s}{u_s} = N_{22} + N_{21}\Delta\left(I - N_{11}\Delta\right)^{-1} N_{12} \qquad (22)$$

where the term $(I - N_{11}\Delta)^{-1}$ can cause instability of the system [30]. The robust stability condition is given by the structured singular value as

$$\mu_\Delta(M) = \frac{1}{\min\left[\bar{\sigma}(\Delta) : \det(I - M\Delta) = 0, \Delta\text{structured}\right]} \qquad (23)$$

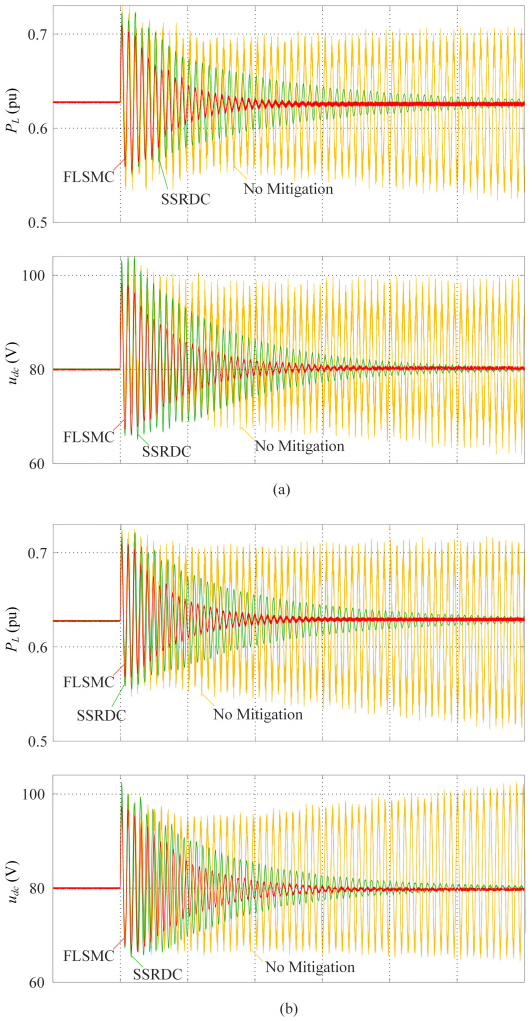

FIGURE 16. Experimental results at 75% compensational level: (a) with +20% variation in GSC filter inductance and resistance; (b) with −20% variation in GSC filter inductance and resistance. (t = 500 ms/div).

The system stability is guaranteed when μ is less than 1. Upper and lower bounds of the SSV are computed utilizing MATLAB as illustrated in Fig. 10. The procedure of evaluating robust stability in this section is demonstrated in Fig. 11.

Figure 10 shows that all values in SSV curves are smaller than 1, which demonstrates the robustness of FLSMC. EMT simulation is performed with ±20% variation in GSC filter inductance (L_{gf}) and GSC filter resistance (R_{gf}). As illustrated in Figs. 12 and 13, parameter perturbation reduces the effectiveness of SSRDC. On the other hand, the effectiveness of the proposed FLSMC in damping SSCI is not much affected by parameter perturbation. This observation validates the SSV analysis.

D. EXPERIMENTAL TEST

As illustrated in Fig. 14, experimental tests are carried out in a 1.5-kW DFIG prototype, and a DC machine is utilized to drive the DFIG. Sensors are connected to the computer via a 1716 Data Acquisition Card. A dSPACEDS 1103 DSP (Texas Instruments) board is used to control GSC and RSC. A TMS320F2812 DSP (Texas Instruments) serves as the microprocessor which generates the control signal for the DFIG. The common dc-link voltage is controlled at 80 V. Experimental tests are performed at compensational level of 75% and 45% respectively, as shown in Fig. 15. Waveforms of active power of transmission line and dc-link voltage demonstrate that the designed FLSMC not only provides desired SSCI damping but mitigates fluctuation of dc-link voltage as well. Furthermore, it is observed from Fig. 15(b) that transient SSCI problem is less severe compared with Fig. 15(a). These observations validate eigenvalue analysis and EMT simulation.

There is a certain degree of DFIG parameter deviation during grid faults. To emulate the condition of the actual DFIG parameter deviation in real time control, the DFIG parameters (L_{gf} and R_{gf}) used in the control laws are varied, but the actual DFIG parameters ($L*gf$ and $R*gf$) are unchanged [31], i.e., $L_{gf} = (1 \pm 0.2)\, L^*_{gf}$ and $R_{gf} = (1 \pm 0.2)\, R^*_{gf}$. The experimental results are illustrated in Fig. 16. It is seen that the proposed FLSMC improves the robustness properties of DFIG under parameter perturbations, which is consistent with the simulation results.

V. CONCLUSION

To overcome the limitations of conventional linear methods, a combined control scheme integrating sliding mode control (SMC) and feedback linearization control (FLC) is proposed to mitigate sub-synchronous control interaction (SSCI) in DFIG-based wind farms. FLC enables the controlled system to be independent of pre-specified operations, and SMC is employed to enhance the insensitiveness to parameter perturbation. To evaluate the performance of the designed feedback-linearized sliding mode controller (FLSMC), small- signal stability analysis and electromagnetic transient simulation are performed at varied operating conditions. The designed FLSMC is observed to demonstrate effectiveness in SSCI mitigation and robustness against parameter uncertainties. Experimental results validate the veracity of the simulation results.

APPENDIX

A. SYSTEM AND CONTROLLER PARAMETERS

See Table 5 and 6.

B. STABILITY OF INTERNAL DYNAMICS

To ensure the stability of the studied system, $\hat{z} = \hat{\phi}(\boldsymbol{x})$ should satisfy the following conditions

$$\begin{cases} L_{g1}\hat{\phi}(\boldsymbol{x}) = 0 \\ L_{g2}\hat{\phi}(\boldsymbol{x}) = 0 \end{cases} \tag{A1}$$

Therefore, we select

$$\begin{aligned} \hat{\phi}(\tilde{x}) &= \hat{\boldsymbol{z}} \\ &= \left[\hat{z}_3\ \hat{z}_4\ \hat{z}_5\ \hat{z}_6\ \hat{z}_7\ \hat{z}_8\ \hat{z}_9\ \hat{z}_{10}\ \hat{z}_{11}\ \hat{z}_{12}\ \hat{z}_{13}\ \hat{z}_{14}\right]^T \\ &= \left[\hat{z}_3\ i_{rq}\ i_{rd}\ i_{sq}\ i_{sd}\ i_q\ i_d\ u_{scq}\ u_{scd}\ \omega_m\ \omega_r\ \gamma\right]^T \end{aligned}$$

TABLE 5. System parameters.

Parameter	Value
Turbine inertia constant H_t/p.u.	2.5
Generator inertia constant H_g/p.u.	0.5
Turbine damping coefficient D_t/p.u.	2.5
Generator damping coefficient D_g/p.u.	0.5
Stiffness coefficient K_s/p.u.	0.15
Stator leakage resistance R_s/p.u.	0.0084
Stator leakage inductance L_s/p.u.	0.167
DC-link capacitance C_{dc}/mF	10
GSC filter resistance R_{gf}/p.u.	0.0015
GSC filter inductance L_{gf}/p.u.	0.15
RSC filter resistance R_{rf}/p.u.	0.0083
RSC filter inductance L_{rf}/p.u.	0.1323
Transformer inductance L_{tr}/p.u.	0.0005
Transmission line resistance R_L/p.u.	0.02
Transmission line resistance L_L/p.u.	0.0016
Compensator capacitance C_{sc}/mF	10
Nominal voltage (line to line) $V_{L\text{-}L}$/V	690

TABLE 6. Controller parameters.

Parameter	Value	Parameter	Value
K_1	0.0001	T_1	0.0500
K_2	0.0000	T_2	0.0050
K_3	0.0001	T_3	0.0250
K_4	0.0001	T_4	0.0025
K_5	0.1000	T_5	0.0500
K_6	1	T_6	100
K_7	0.1000	T_7	0.0500
K_8	1	T_8	100
K_p	30		

where $\hat{z}_3$ is expressed as

$$\hat{z}_3 = \frac{1}{2}L_{gf}i_{gq}^2 + \frac{1}{2}L_{gf}i_{gd}^2 + \frac{1}{2}C_{dc}u_{dc}^2 \tag{A2}$$

Since $\tilde{z}_1 = \tilde{z}_2 = 0$ at steady state, $\tilde{z}_3$ is written as

$$\hat{z}_3 = \frac{1}{2}L_{gf}i_{gd}^2 \tag{A3}$$

The dynamics of $\hat{z}_3$ is obtained

$$\frac{\mathrm{d}}{\mathrm{d}t}\hat{z}_3 = L_f\hat{\phi}\left(\tilde{x}\right) = L_{gf}i_{gd}\left(\omega_1 i_{gq} - \frac{R_{gf}}{L_{gf}}i_{gd} - \frac{u_{gd}}{L_{gf}}\right) \tag{A4}$$

Considering $u_{gd} = 0$ and $\tilde{z}_1 = i_{gq} = 0$, following expression is derived

$$\frac{\mathrm{d}}{\mathrm{d}t}\hat{z}_3 = -R_{gf}i_{gd}^2 \tag{A5}$$

Based on (A3), (A4), and (A5), the simplified dynamics of $\hat{z}_3$ is expressed as

$$\frac{\mathrm{d}}{\mathrm{d}t}\hat{z}_3 = -\frac{2R_{gf}}{L_{gf}}\hat{z}_3 \tag{A6}$$

Equation (A6) indicates a stable system, and dynamics of remaining states are obtained

$$\frac{\mathrm{d}}{\mathrm{d}t}\hat{z}_i = L_f\hat{\phi}\left(\boldsymbol{x}\right) = 0; \quad i = 4, 5, \ldots, 14 \tag{A7}$$

Therefore, the feedback linearization method is implementable to the studied system.

C. EXPRESSION OF $g(x)$ AND $f(x)$

$$g\left(\boldsymbol{x}\right) = \begin{bmatrix} u_{dc}/L_{gf} & 0 \\ 0 & u_{dc}/L_{gf} \\ -i_{gq}/C_{dc} & -i_{gd}/C_{dc} \\ 0 & 0 \\ 0 & 0 \\ 0 & 0 \\ 0 & 0 \\ 0 & 0 \\ 0 & 0 \\ 0 & 0 \\ 0 & 0 \\ 0 & 0 \\ 0 & 0 \\ 0 & 0 \end{bmatrix}$$

$$f\left(\boldsymbol{x}\right) = \begin{bmatrix} -\omega_1 i_{gd} - \frac{R_{gf}}{L_{gf}}i_{gq} - \frac{u_{gq}}{L_{gf}} \\ \omega_1 i_{gq} - \frac{R_{gf}}{L_{gf}}i_{gd} - \frac{u_{gd}}{L_{gf}} \\ i_{dc}/C_{dc} \\ \omega_1 i_{rd} - \frac{R_{rf}}{L_{rf}}i_{rq} - \frac{u_{rq}}{L_{rf}} \\ -\omega_1 i_{rq} - \frac{R_{rf}}{L_{rf}}i_{rd} - \frac{u_{rd}}{L_{rf}} \\ -\omega_1 i_{sd} + \frac{R_s}{L_s}i_{sq} + \frac{u_{sq}}{L_s} \\ \omega_1 i_{sq} + \frac{R_s}{L_s}i_{sd} + \frac{u_{sd}}{L_s} \\ -\omega_1 i_d + \frac{R_L}{L_L}i_q + \frac{1}{L_L}\left(u_q - u_{scq} - e_q\right) \\ \omega_1 i_q + \frac{R_L}{L_L}i_d + \frac{1}{L_L}\left(u_d - u_{scd} - e_d\right) \\ -\omega_1 u_{scd} + i_q/C_{sc} \\ \omega_1 u_{scq} + i_d/C_{sc} \\ \left(T_{ae} - K_s\gamma - D_t\omega_m\right)/2H_t \\ \left(K_s\gamma - T_e - D_g\omega_r\right)/2H_g \\ 2\pi f\left(\omega_m - \omega_r/N_g\right) \end{bmatrix}$$

REFERENCES

[1] G. D. Irwin, A. K. Jindal, and A. L. Isaacs, "Sub-synchronous control interactions between type 3 wind turbines and series compensated AC transmission systems," in *Proc. IEEE PES Gen. Meeting*, Detroit, MI, USA, Jul. 2011, pp. 1–6.

[2] H. Cho, S. Oh, S. Nam, and B. Lee, "Non-linear dynamics based sub-synchronous resonance index by using power system measurement data," *IET Gener., Transmiss., Distrib.*, vol. 12, no. 17, pp. 4026–4033, Sep. 2018.

[3] L. Gross, "Sub-synchronous grid conditions: New event, new problem, and new solutions," in *Proc. 37th Annu. Western Protective Relay Conf.*, Spokane, WA, USA, 2010, pp. 1–19.
[4] K. Narendra *et al.*, "New microprocessor based relay to monitor and protect power systems against sub-harmonics," in *Proc. IEEE Elect. Power Energy Conf.*, Winnipeg, MB, Canada, Oct. 2011, pp. 438–443.
[5] L. Wang, X. Xie, Q. Jiang, H. Liu, Y. Li, and H. K. Liu, "Investigation of SSR in practical DFIG-based wind farms connected to a series-compensated power system," *IEEE Trans. Power Syst.*, vol. 30, no. 5, pp. 2772–2779, Sep. 2015.
[6] H. Liu and X. Xie, "Impedance network modeling and quantitative stability analysis of sub-/super-synchronous oscillations for large-scale wind power systems," *IEEE Access*, vol. 6, pp. 34431–34438, Jun. 2018.
[7] X. Xie, X. Zhang, H. Liu, H. Liu, Y. Li, and C. Zhang, "Characteristic analysis of subsynchronous resonance in practical wind farms connected to series-compensated transmissions," *IEEE Trans. Energy Convers.*, vol. 32, no. 3, pp. 1117–1126, Sep. 2017.
[8] A. E. Leon, "Integration of DFIG-based wind farms into series-compensated transmission systems," *IEEE Trans. Sustain. Energy*, vol. 7, no. 2, pp. 451–460, Apr. 2016.
[9] A. E. Leon and J. A. Solsona, "Sub-synchronous interaction damping control for DFIG wind turbines," *IEEE Trans. Power Syst.*, vol. 30, no. 1, pp. 419–428, Jan. 2015.
[10] P. Li, J. Wang, F. Wu, and H. Li, "Nonlinear controller based on state feedback linearization for series-compensated DFIG-based wind power plants to mitigate sub-synchronous control interaction," *Int. Trans. Electr. Energ. Syst.*, vol. 29, no. 1, p. e2682, Jan. 2019.
[11] H. A. Mohammadpour and E. Santi, "SSR damping controller design and optimal placement in rotor-side and grid-side converters of series-compensated DFIG-based wind farm," *IEEE Trans. Sustain. Energy*, vol. 6, no. 2, pp. 388–399, Apr. 2015.
[12] P. Li, J. Wang, L. Xiong, and F. Wu, "Nonlinear controllers based on exact feedback linearization for series-compensated DFIG-based wind parks to mitigate sub-synchronous control interaction," *Energies*, vol. 10, no. 8, p. 1182, Aug. 2017.
[13] D. H. R. Suriyaarachchi, U. D. Annakkage, C. Karawita, D. Kell, R. Mendis, and R. Chopra, "Application of an SVC to damp sub-synchronous interaction between wind farms and series compensated transmission lines," in *Proc. IEEE PES Gen. Meeting*, Jul. 2012, pp. 1–6.
[14] A. Moharana, R. K. Varma, and R. Seethapathy, "SSR alleviation by STATCOM in induction-generator-based wind farm connected to series compensated line," *IEEE Trans. Sustain. Energy*, vol. 5, no. 3, pp. 947–957, Jul. 2014.
[15] X. Wu, S. Feng, P. Jiang, G. Xu, and X. Yang, "An SSR multichannel damping control scheme for TCSC considering multiple operating conditions," *Int. Trans. Elect. Energy Syst.*, vol. 26, no. 12, pp. 2759–2773, Dec. 2016.
[16] J. Khazaie, M. Mokhtari, S. Badkuvi, M. Khalilian, and D. Nazarpour, "Sub-synchronous resonance mitigation via distributed power flow controller," *Int. Trans. Electr. Energy Syst.*, vol. 23, no. 6, pp. 751–766, Jun. 2013.
[17] U. Malhotra and R. Gokaraju, "An add-on self-tuning control system for a UPFC application," *IEEE Trans. Ind. Electron.*, vol. 61, no. 5, pp. 2378–2388, May 2014.
[18] H. A. Mohammadpour and E. Santi, "Modeling and control of gate-controlled series capacitor interfaced with a DFIG-based wind farm," *IEEE Trans. Ind. Electron.*, vol. 62, no. 2, pp. 1022–1033, Feb. 2015.
[19] L. Fan and Z. Miao, "Mitigating SSR using DFIG-based wind generation," *IEEE Trans. Sustain. Energy*, vol. 3, no. 3, pp. 349–358, Jul. 2012.
[20] H. Liu, X. Xie, J. He, H. Liu, and Y. Li, "Damping DFIG-associated SSR by adding subsynchronous suppression filters to DFIG converter controllers," in *Proc. IEEE Power Energy Soc. Gen. Meeting*, Boston, MA, USA, Jul. 2016, pp. 1–5.
[21] P.-H. Huang, M. El Moursi, W. Xiao, and J. Kirtley, "Subsynchronous resonance mitigation for series-compensated DFIG-based wind farm by using two-degree-of-freedom control strategy," *IEEE Trans. Power Syst.*, vol. 30, no. 3, pp. 1442–1454, May 2015.
[22] M. Ghafouri, U. Karaagac, H. Karimi, S. Jensen, J. Mahseredjian, and S. O. Faried, "An LQR controller for damping of subsynchronous interaction in DFIG-based wind farms," *IEEE Trans. Power Syst.*, vol. 32, no. 6, pp. 4934–4942, Nov. 2017.
[23] X. Xie, H. Liu, and Y. Han, "Coordinated design of supplementary excitation damping controller and voltage-sourced converter based generator terminal subsynchronous damping controller for subsynchronous resonance suppression: A case study," *Elect. Power Compon. Syst.*, vol. 44, no. 5, pp. 565–577, Feb. 2016.
[24] J. Hu, Z. Wang, H. Gao, and L. K. Stergioulas, "Robust sliding mode control for discrete stochastic systems with mixed time delays, randomly occurring uncertainties, and randomly occurring nonlinearities," *IEEE Trans. Ind. Electron.*, vol. 59, no. 7, pp. 3008–3015, Jul. 2012.
[25] L. Xiong, J. Wang, X. Mi, and M. W. Khan, "Fractional order sliding mode based direct power control of grid-connected DFIG," *IEEE Trans. Power Syst.*, vol. 33, no. 3, pp. 3087–3096, May 2018.
[26] J. Hu, Z. Wang, Y. Niu, and H. Gao, "Sliding mode control for uncertain discrete-time systems with Markovian jumping parameters and mixed delays," *J. Franklin Inst.*, vol. 351, no. 4, pp. 2185–2202, Apr. 2014.
[27] L. Fan, R. Kavasseri, Z. L. Miao, and C. Zhu, "Modeling of DFIG-based wind farms for SSR analysis," *IEEE Trans. Power Del.*, vol. 25, no. 4, pp. 2073–2082, Oct. 2010.
[28] M. A. Mahmud, H. R. Pota, and M. J. Hossain, "Dynamic stability of three-phase grid-connected photovoltaic system using zero dynamic design approach," *IEEE J. Photovolt.*, vol. 2, no. 4, pp. 564–571, Oct. 2012.
[29] P. Kundur, *Power System Stability and Control*. New York, NY, USA: McGraw-Hill, 1994.
[30] S. Sumsurooah, M. Odavic, and S. Bozhko, "A modeling methodology for robust stability analysis of nonlinear electrical power systems under parameter uncertainties," *IEEE Trans. Ind. Appl.*, vol. 52, no. 5, pp. 4416–4425, Sep. 2016.
[31] D. Zhu, X. Zou, S. Zhou, W. Dong, Y. Kang, and J. Hu, "Feedforward current references control for DFIG-based wind turbine to improve transient control performance during grid faults," *IEEE Trans. Energy Convers.*, vol. 33, no. 2, pp. 670–681, Jun. 2018.

PENGHAN LI received the B.S. degree in electrical engineering from the Harbin Institute of Technology, Harbin, China, in 2016. He is currently pursuing the Ph.D. degree in electrical engineering with the School of Electronic Information and Electrical Engineering, Shanghai Jiao Tong University. His research interests include power system nonlinear control and renewable power generation.

JIE WANG received the M.S. degree from North China Electric Power University, Baoding, China, in 1991, and the Ph.D. degree from Northeastern University, Shenyang, China, in 1998. From 1982 to 2002, he worked on the fields of industrial automation and power system automation. From 1999 to 2001, he was with Shanghai Jiao Tong University, Shanghai, China, where he was involved in the research work on the nonlinear control and the Hamiltonian system. He is currently working in the field of power system stability and control.

LINYUN XIONG was born in Chongqing, China, in 1993. He received the B.S. degree in electrical engineering from Sichuan University, Chengdu, China, in 2015, and the Ph.D. degree from the School of Electronic Information and Electrical Engineering, Shanghai Jiao Tong University, Shanghai, China, in 2019. He is currently a Lecturer with the School of Electrical Engineering, Chongqing University, Chongqing. His research interests include power system nonlinear control and Hamiltonian system.

MEILING MA received the B.S. and M.S. degrees from Nanjing Normal University, Nanjing, China, in 2012 and 2015, respectively. She is currently pursuing the Ph.D. degree with the School of Electronic Information and Electrical Engineering, Shanghai Jiao Tong University. From 2015 to 2017, she was with the Taizhou College, Nanjing Normal University, Taizhou, China, where she was worked on the field of nonlinear dynamics of power system. Her research interests include the power system transient stability and the Hamilton realization of power systems.